Tsunami Force Estimation on Selected California Coastal Bridges

Mohsen Azadbakht [1] and Solomon C. Yim [2]

Abstract

Tsunami force time histories are simulated for three selected California coastal bridges. The tsunami flow field input including water free-surface elevation and horizontal velocity components were provided by the California Department of Transportation (Caltrans). Tsunami water free-surface maximum elevations are 5, 10, 15, 20, and 25 feet above bridge elevation yielding five tsunami flow conditions for each bridge. For each tsunami flow condition, the force time histories are calculated for four time periods: a) initial impact, b) duration when the maximum water velocity occurs, c) duration when the maximum momentum flux (H*V2) occurs, and d) duration when the maximum elevation times velocity (H*V) occurs. The resulting horizontal and vertical forces and overturning moments are analyzed and compared for the selected time periods for each tsunami flow condition. From the numerical simulations, it is found that the resulting maximum horizontal force always increases by increasing the water surface elevation (with corresponding scaled velocities). This increase is not significantly large for box-girder bridges. The maximum vertical forces can increase or decrease based on bridge geometry and water velocity while overtopping the bridge. The calculated horizontal and vertical forces are about the same for higher water elevations meaning that the increase in the water level no longer changes the resulting forces significantly. In almost all the cases studied here the resulting downward force caused by water overtopping the bridge is larger than the uplift force. In most of the cases the maximum vertical force occurs in the initial impact time period while maximum horizontal force occurs in the time period containing maximum momentum flux, velocity, and elevation times velocity. Vertical forces acting on bridge superstructures are found to be approximately 2 to 4 times larger than corresponding horizontal forces. Finally, it is essential that the results and conclusions derived from this and similar numerical studies (including those of the Oregon coastal bridges over the past few years) be validated by large-scale experiments to assess their predictive capability and ranges of variability.

Introduction

Tsunamis have caused significant damage to coastal communities in recent years. The 2011 Great East Japan Earthquake and resulting Tohoku Tsunami destroyed many infrastructures along Japan's east coast including bridge superstructures (Iemura, 2005; Robertson et al., 2011; Yashinsky 2012). Figure 1 shows an example of failure of the connections attaching the bridge superstructure to substructure during the 2011 Japan earthquake and tsunami. Highway bridges, as an important part of transportation system, have a significant role in maintaining access to coastal communities after a tsunami. Therefore, tsunami-resistant design of these superstructures is crucial. Although the scientific community has been interested in behavior of bridges during hurricanes and storm surges over the years (e.g. Douglass et al., 2006; Robertson et al., 2007a

---

[1] Graduate Research Assistant, School of Civil and Construction Engineering, Oregon State University, Corvallis, OR, USA

[2] Professor, School of Civil and Construction Engineering, Oregon State University, Corvallis, OR, USA

and b; Padgett et al., 2008) not many studies have been conducted regarding measuring tsunami forces on bridge superstructures. The interest of Oregon Department of Transportation (ODOT) in predicting tsunami forces on bridge superstructures led to a series of numerical studies at Oregon State University (OSU). Nimmala (Nimmala et al. 2006) computed the tsunami loads on Spencer Creek Bridge. Cheung (Cheung et al. 2011) developed a set of tsunami scenarios for probabilistic design of bridge superstructures. These tsunami scenarios were used to numerically estimate the tsunami loading on four bridges located on Highway 101 in the Siletz Bay area on the Oregon Coast (Yim et al. 2011).

This paper presents preliminary results of an ongoing study on numerically simulating tsunami forces on three selected bridge superstructures along California coast line. The locations of these bridges are shown in Figure 2. Tsunami flow conditions for these three selected bridges were provided by the California Department of Transportation (Caltrans). These tsunami flow condition data sets contain water free-surface elevation and horizontal velocity components as a boundary condition input in finite element model (FEM) in order to calculate the fluid flow field surrounding the bridge and the horizontal and vertical forces time histories as well as overturning moment acting on bridge superstructures due to tsunami loading.

Figure 1. Utatsu Bridge failure during 2011 Japan earthquake and tsunami (Photo by Yim)

Tsunami Flow Field Boundary Condition Generation and Critical Time Periods

Tsunami flow fields including water free-surface elevation and horizontal velocity components near the bridge sites were provided by Caltrans. These tsunami flow fields were developed for different return periods up to 2500 years based on distant tsunami sources, and were calculated based on earthquakes sources only. In this method deformation and displacement of the ocean floor caused by earthquake are used to compute the change in water surface elevation. Long wave approximation is used to model the propagation of the tsunami towards the coast. According to this theory the vertical acceleration of water in negligible compared to gravity acceleration resulting in uniform velocity in water column which travels in horizontal direction. The finite difference method is used to solve the equations of motion and continuity (California Tsunami Hazard, 2010).

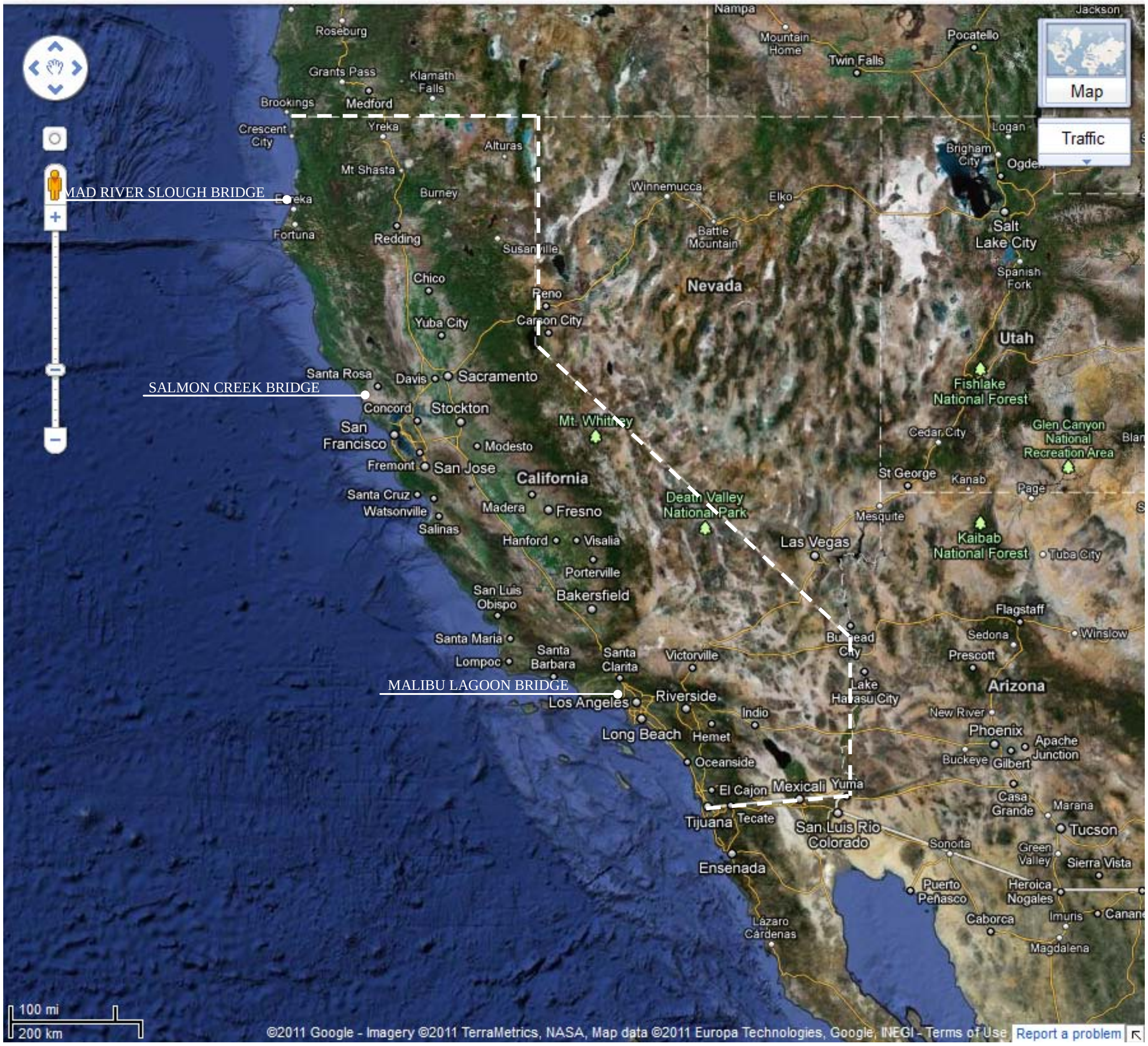

Figure 2. Locations of selected bridges along California coast line (Source: Google Maps)

The time histories of tsunami water free-surface elevation and horizontal velocity components near the location of three selected bridges were provided by Caltrans. This information is used as the boundary condition of a fluid flow field surrounding the bridge superstructure. (This boundary is set sufficiently far away from the superstructure such that the domain of influence of the presence of the superstructure does not overlap the input boundary but as close as possible to maximize the tsunami loads and minimize the computational domain.)

Since the water free-surface elevations in provided data sets were lower than the elevation of the bridges, it was decided that the (maximum) water free-surface elevation be scaled up to 5, 10, 15, 20, and 25 feet above bridge elevation, and the rest of the water free-surface elevation time history were scaled up accordingly. The tsunami velocity components profile at the boundary was scaled using square root of the scale factor used to increase the water surface elevation (based on dimensional analysis and scaling theory). Figure 3 shows, for example, the tsunami free-surface elevation and the water velocity component normal to the bridge superstructure at the location of the Salmon Creek Bridge.

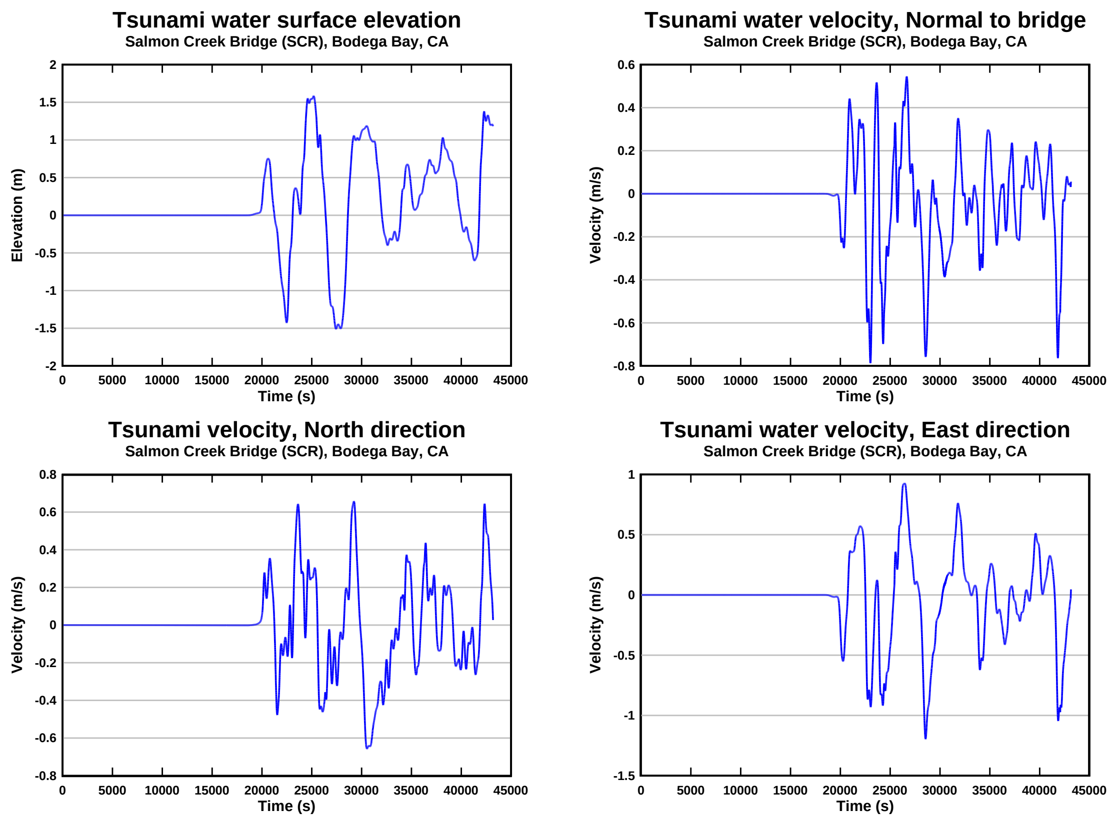

Figure 3. Tsunami surface elevation and water velocity at the location of the Salmon Creek Bridge

Tsunami flow durations are usually on the order of hours, thus in order to capture the behavior of the structure under several impacts and inundations through the whole process, multiple time durations should be analyzed in detail. Since it is impractical to perform a large-domain computational fluid dynamics (CFD) analysis from beginning to the end for such a long duration, it was decided to perform the simulations for a set of time periods representing the most critical cases such that the studied time periods essentially cover all the important features of the entire tsunami load duration. Followings are the time periods studied:

a. initial impact
b. the load duration when maximum water velocity (V) occurs
c. the load duration when the maximum momentum flux ($H*V^2$) occurs; and
d. the load duration when the maximum elevation times velocity (H*V) occurs.

Note that H is the tsunami water free-surface elevation and V is the tsunami water free-surface velocity. Initial impact time period refers to a load duration that tsunami water free-surface elevation reaches the elevation of the bridge inducing the first interaction between water and the seaward side of the bridge cross-section. Since there are several initial impacts during a tsunami due to different number of waves hitting the bridge superstructure during the entire tsunami, the time period that contained the highest velocity was selected to perform the CFD analysis. The maximum water velocity duration represents a time period in which the water reaches its highest velocity during the tsunami. The maximum momentum flux (H*V2) and maximum elevation times velocity (H*V) refer to the time periods in which the maximum momentum flux (H*V2) and maximum elevation times velocity (H*V) were recorded, respectively. For cases that initial impact on the bridge superstructure happened not long before that the time period that maximum water velocity, momentum flux (H*V2), and elevation times velocity (H*V) happened a single model was utilized to calculate the resulting forces induced by tsunami on the bridge superstructure from initial impact to total submergence of the structure. In other cases separate analyses were performed. Figure 4a, for example, shows the scaled water free-surface elevation compared to the bridge elevation. A sample time period chosen to study four different time periods mentioned above is provided in Figure 4b.

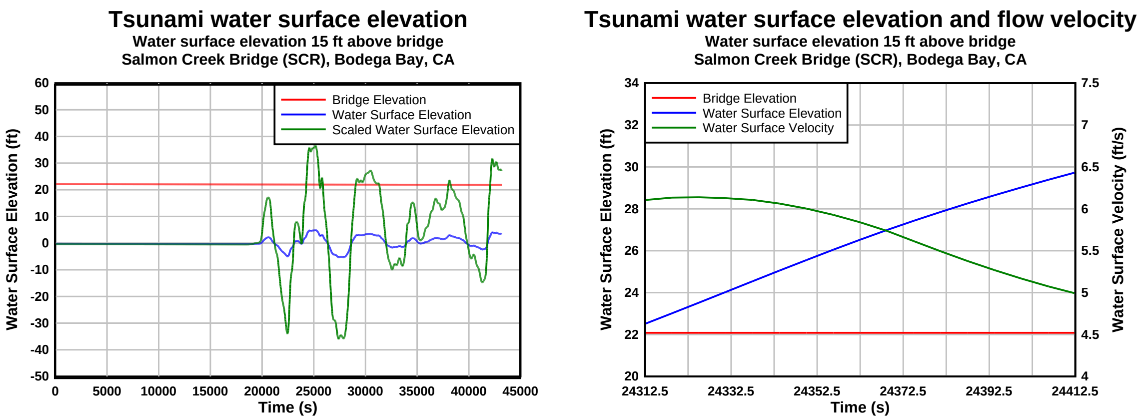

a. b.

Figure 4a and b. Scaled water surface elevation and selected time period

Numerical Modeling

A finite element analysis (FEA) code LS-DYNA was used to perform the CFD analysis and calculate the horizontal and vertical forces on selected bridges due to tsunami loading. The program solves the Navier-Stokes (N-S) equations to obtain the pressure and consequently force on the structure. An arbitrary Lagrangian-Eulerian (ALE) formulation was used to track the fluid particles on the fluid free surface. The advantages of using this model over the other available CFD analysis codes is its ability to solve (N-S) equations and accurately model multi-physics contact and impact instead of potential flow equations which widely used in the ocean and coastal engineering community. The ability to solve (N-S) equations allows the model to capture all the effects related to fluid viscosity and rotation of the fluid particles which are neglected in potential theory based codes. This feature, for example, makes the program able to model wave breaking and fluid impact on the structure, which are crucial in modeling the tsunami and its effects on the structure. Another advantage is that LS-DYNA is capable of modeling hydro-elasticity, meaning that the elastic response of structures under fluid-induced loadings and likewise the influence of the structure motion on the fluid (i.e. the tsunami flow field) can be studied while most other currently available CFD codes treat the structure as a rigid body. The ability to solve the NS equations along with being capable of modeling hydro-elasticity are unique features that differentiate this code from most other commercially available CFD codes (LS-DYNA 2010). Figure 5 shows the different parts of the FE model domain of the Mad River Slough Bridge. The two-dimensional (2D) fluid-structure interaction model consists of two parts: a) a fluid part which includes both water and air domains and b) a bridge superstructure. Solid brick elements are used to model the whole domain. In this study, the bridge superstructure is modeled as a rigid body held by elastic supports. Pin and roller reaction supports are used to create sufficient constraints to make the structure determined and stable. Appropriate elastic modulus and Poison ratio representing the reinforced concrete material are used for the bridge superstructure. Both water and air materials are modeled as compressible materials. Appropriate densities, viscosity coefficients, and equation of states are considered for both water and air. The value of sound speed is reduced judiciously in the simulations to decrease the run time without sacrificing the accuracy of the results. The input flow boundary condition is modeled as a water column at the left boundary of domain where the tsunami velocity profile is applied.

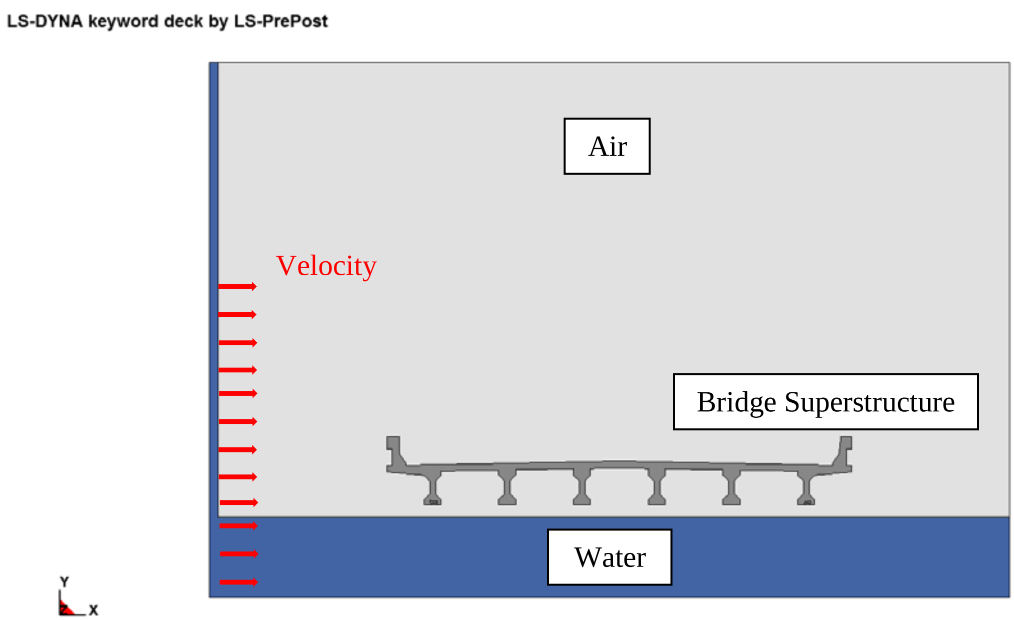

Figure 5. Finite Element Model of Mad River Slough Bridge Superstructure

The resulting overturning moment is computed about the right end support, flow is moving from left to right, via multiplying horizontal and vertical forces by corresponding moment arms. It is assumed that the horizontal and vertical forces are acting at the center of the mass of the structure. The positive directions used to calculate the time history of horizontal and vertical forces are shown in Figure 6.

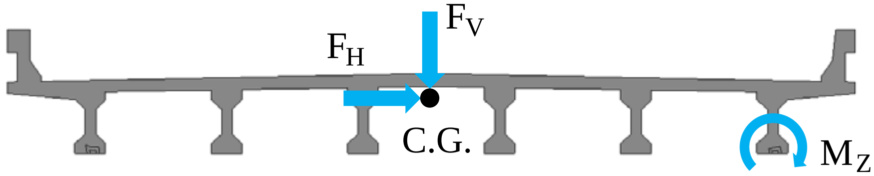

Figure 6. Positive directions used to calculate the time history of horizontal and vertical forces and overturning moments

Results and Discussion

The results of the FE analyses performed to calculate the tsunami force on the three selected bridges are presented in this section. The three bridges studied here are: Mad River Slough Bridge, Salmon Creek Bridge, and Malibu Lagoon Bridge.

1. Mad River Slough Bridge

The Mad River Slough Bridge is a deck-girder bridge with a reference elevation 8 foot – 8 inches above the mean sea level (MSL). A total of nine simulations were performed in order to study the tsunami. For the (maximum) tsunami water free-surface elevation 5 ft above the bridge, all the four different critical time periods mentioned in the above section occur at the same time, thus requiring only one simulation to cover all four periods. For the other four water elevations (10, 15, 20, and 25 ft), two simulations were performed for each water elevation, with one for the initial impact and the other for maximum momentum flux, H*V, and velocity time periods as all these three occur at the same time. It should be mentioned that in order to interpret the results from the different time periods except the initial impact, the first 10 to 20 seconds are neglected as this is when the initial impact occurs. Since maximum water elevation might occur at the different time than the maximum momentum flux, H*V, and velocity, the water surface elevation should not be expected to be at exactly, for example, 15 ft above the bridge in the simulation representing the scaled water elevation of 15 ft above bridge elevation. For this particular bridge the time that maximum momentum flux, H*V, and velocity occur is close to that of maximum water elevation creating a large hydrostatic pressure and consequently large horizontal force. A set of screen captures of initial impact time period simulation of Mad River Slough Bridge for a water free-surface elevation of 15 ft above bridge elevation is provided in Figure 7.

Three different aspects of these simulations are discussed here:

- Resulting force time history obtained in each simulation
- Comparison between different force time histories obtained from different time periods
- Comparison between different force time histories obtained from different water elevations

Tsunami force time histories obtained from all nine simulations for this bridge can be classified in two categories:

The first category is associated with the simulation of tsunami impact in the initial impact time period. Figure 8a and b show the tsunami force time history on the Mad River Slough Bridge for the scaled tsunami water free-surface elevation of 15 ft above bridge elevation. The resulting horizontal and vertical forces for two time periods are provided. Figure 8.a shows a sudden increase in both horizontal and vertical forces due to first impact followed by a relatively constant drag force. During the initial impact time period the tsunami water free-surface elevation has just reached to the elevation of the bridge. Tsunami flow velocity for all five initial impact time periods has been recorded between 5 to 7 (ft/s) resulting in 9 to 10 (Kip/ft) horizontal force on the bridge superstructure. Corresponding downward vertical forces on the bridge superstructure were found to increase from 13.6 to 28 (Kip/ft) by increasing the tsunami water surface elevation.

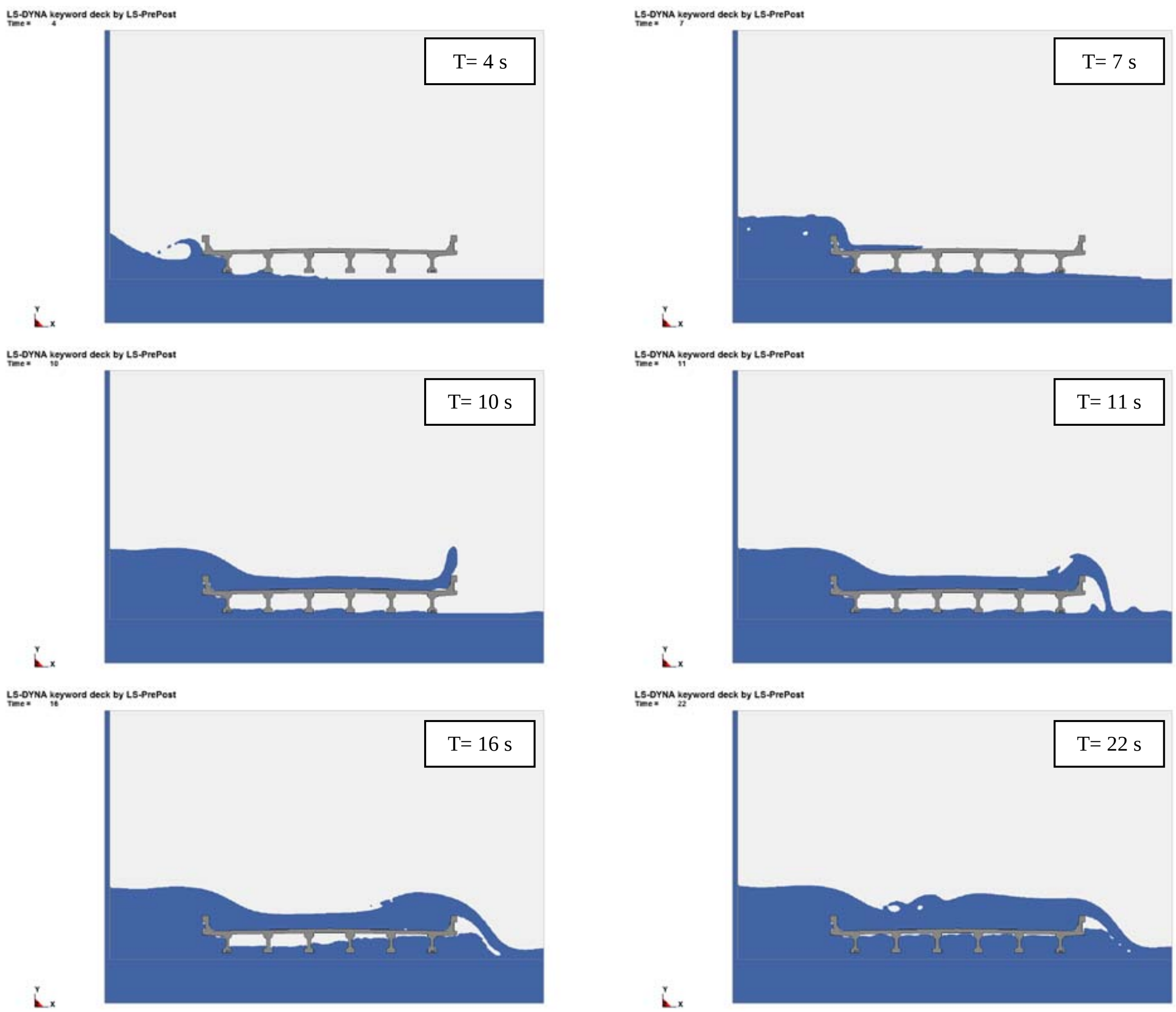

Figure 7. Screen captures of Mad River Bridge, Water surface elevation 15 ft above bridge elevation, Initial impact time period

The second category is related to the maximum momentum flux, H*V, and velocity time periods. For these time periods, according to Figure 8.b, after the first impact there is a relatively constant horizontal force and decreasing downward vertical force toward the end of the simulation when the bridge is completely inundated. This reduction in vertical force is because of total submergence of the bridge creating the uplift force which reduces the slamming force caused by water overtopping the bridge. Since this downward vertical force is caused by the water overtopping the bridge, by increasing the tsunami water surface elevation the amount of the water which overtops the bridge increases resulting in higher downward vertical force. This process continues until the water elevation in high enough and the air pockets trapped under the bridge deck were collapsed that increasing the water level no longer creates significantly larger vertical forces. Figure 9 shows the maximum horizontal and downward vertical force for five different water elevations. According to the figure, the maximum force gradually increases with increasing tsunami water free-surface elevation for both horizontal and vertical forces. Note that the resulting forces are practically identical for three higher scaled elevations (15, 20, and 25 ft above bridge elevation). Uplift forces were not recorded in any of the cases except for the one with water elevation 5 ft above bridge. This uplift force was recorded at the end of the simulation. It can be concluded that, because of the low water elevation (5 ft above bridge elevation), the downward velocity of water overtopping the bridge is low, leading to a relatively small downward vertical force, this downward vertical force was gradually overcome by uplift force as the whole bridge started to be inundated toward the end of the simulation. This behavior is different for the higher water free-surface elevations as the resulting force due to water overtopping and slamming the bridge is much larger than the uplift force. It is also observed that the maximum horizontal and vertical load occur in time period related to maximum momentum flux, H*V, and velocity compared to initial impact time period.

2. Salmon Creek Bridge

The Salmon Creek Bridge is a box-girder bridge with elevation approximately 15 foot - 9 inches above MSL. Seven simulations were performed and analyzed for this bridge. For the three tsunami water free-surface elevations of 5, 10, 15 ft above bridge all four different time periods occur at the same time requiring three simulations to calculate tsunami force time histories for these three water elevations. For the water elevations of 20 and 25 ft above bridge elevation the initial impact is modeled separately since it occurs at the different time. A set of screen captures of the simulation of Salmon Creek Bridge for water surface elevation of 15 ft above bridge elevation are provided in Figure 10.

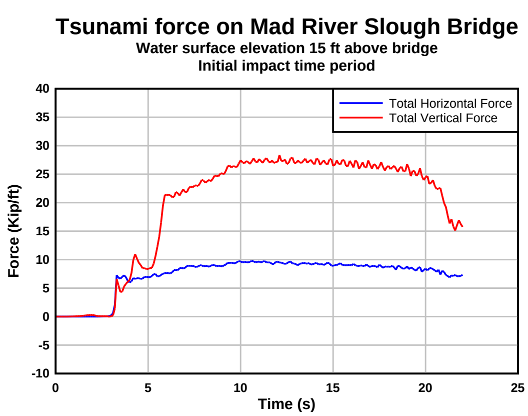

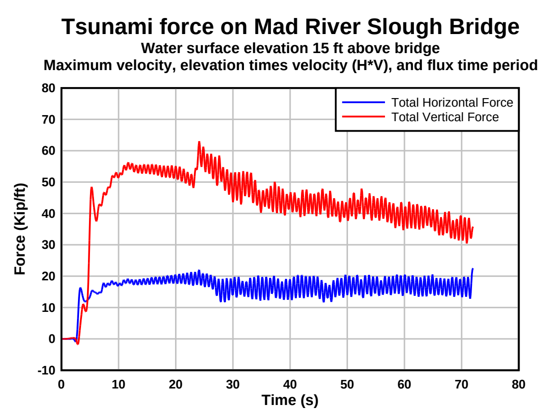

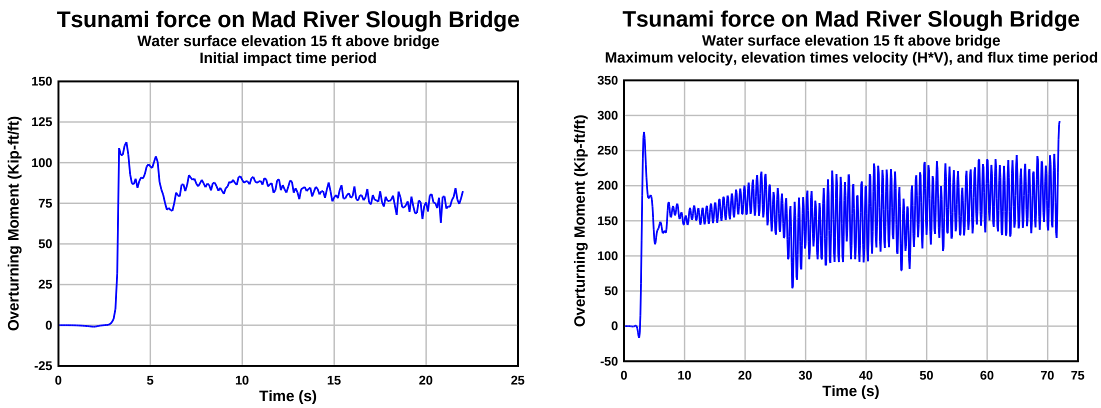

a. b.

Figure 8a and b. Tsunami force time history on the Mad River Slough Bridge, Water surface elevation 15 ft above bridge elevation. a) Initial impact time period and b) maximum momentum flux, H*V, and velocity time period

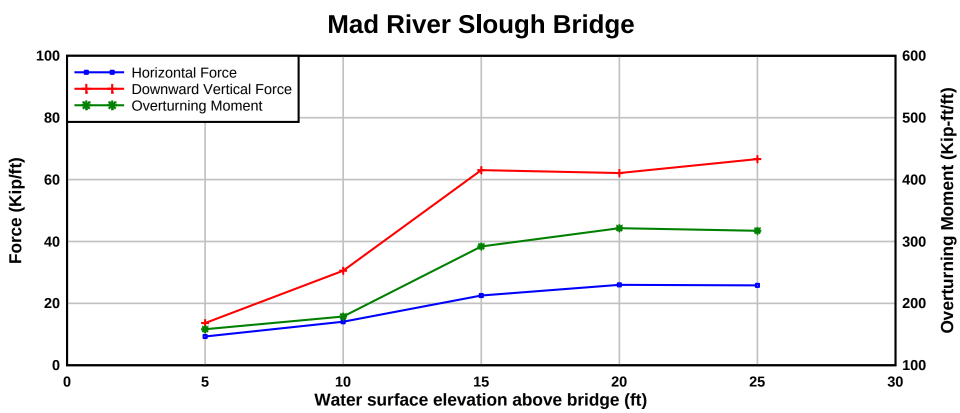

Figure 9. Maximum horizontal and vertical forces and overturning moment on Mad River Slough Bridge for five different water elevations

Tsunami force time history on the Salmon Creek Bridge for the scaled tsunami water free-surface elevation of 15 ft above the bridge elevation is provided in Figure 11. By comparing the time histories of horizontal and vertical forces, it is found that the behavior is almost the same for all different time periods. As observed in the figure, there is a sudden increase in both horizontal and vertical forces due to first impact followed by a relatively constant drag force. Initial impact forces are found to be 10% to 30% higher than the corresponding drag forces. Note that this is a downward force resulting from the water overtopping the bridge. Uplift forces were not predicted in any of simulation cases. It is observed that for the cases including the initial impact both maximum horizontal and vertical forces occur during the impact on the second bridge rail (farther rail at right end). It is also concluded that the horizontal force is larger during the maximum momentum flux, HV and velocity time period compared to the initial impact time period but the vertical force is larger during the initial impact time period. Tsunami loading on this bridge is significantly influenced by the relatively tall end barriers and rails compared to the thickness of the bridge deck. It is also observed that the maximum horizontal force gradually increases by increasing the water surface elevation. Maximum downward vertical force decreases by increasing the water surface elevation except for the last one (water surface elevation 25 ft above bridge). It can be observed in Figure 12 that the amount of maximum downward vertical force is almost identical for water surface elevations 10, 15, 20, and 25 ft above bridge elevation. By comparing the screen captures of the bridge during the simulation when the maximum vertical force occurred, it is concluded that the difference between maximum force for water surface elevation 5 ft above bridge and the other four elevations is due to larger amount of water accumulated on the bridge between the rails. For the case of water surface elevation 5 ft above bridge elevation, the flow velocity is relatively slow so that there is enough time for water to fill up the space between the rails on the bridge. Note that during the initial impact on the bridge since the bridge is not fully inundated this accumulation of water on the bridge creates more downward vertical force. For other elevations, because the velocity is higher, the vertical force is mostly influenced by the impact on the farther rail (right end rail) in addition to downward force created by the water overtopping the bridge. It should be mentioned that since the vertical force is much larger than the horizontal force the overturning moment is controlled by this force.

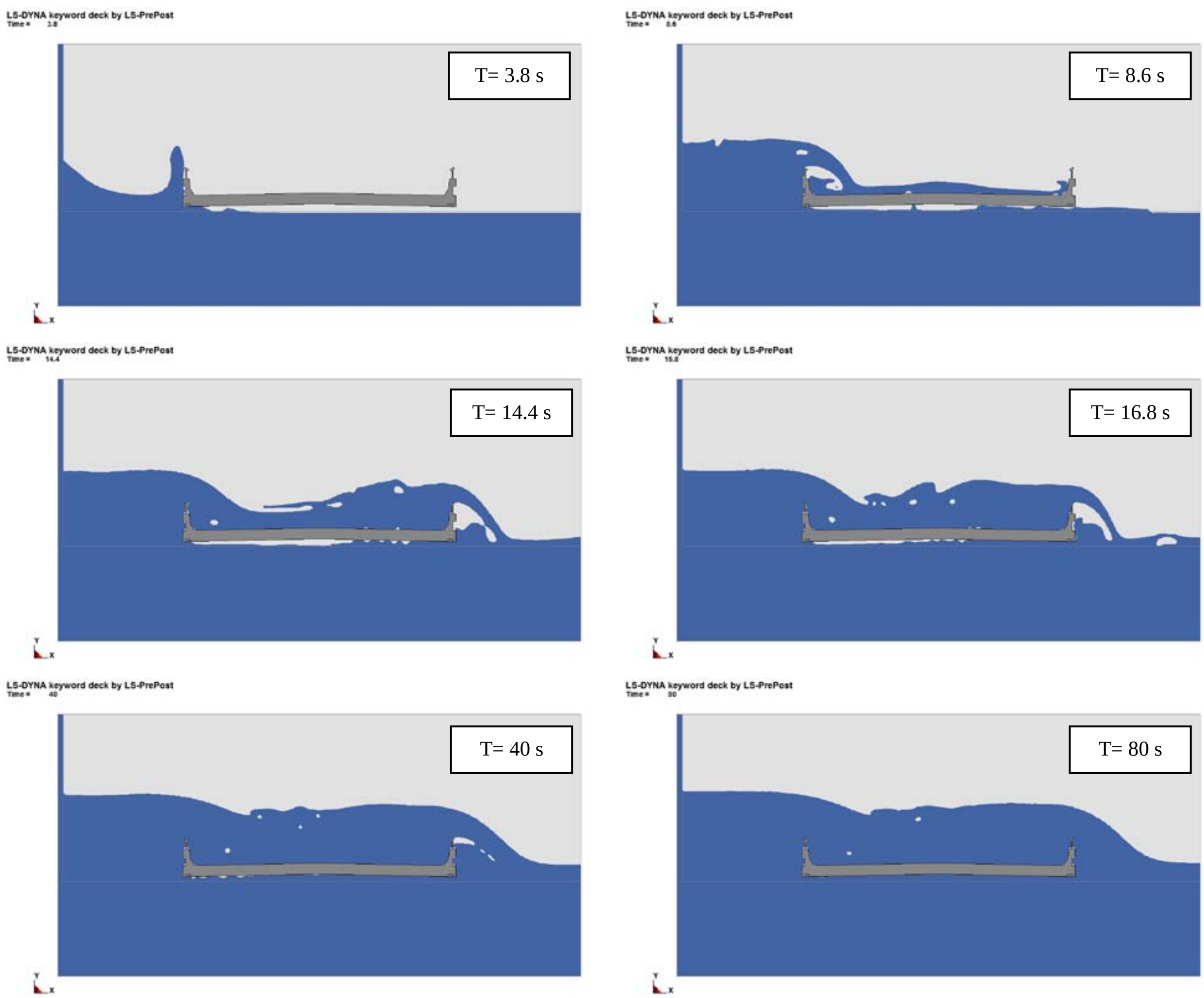

Figure 10. Screen captures of Salmon Creek Bridge, Water surface elevation 15 ft above bridge elevation

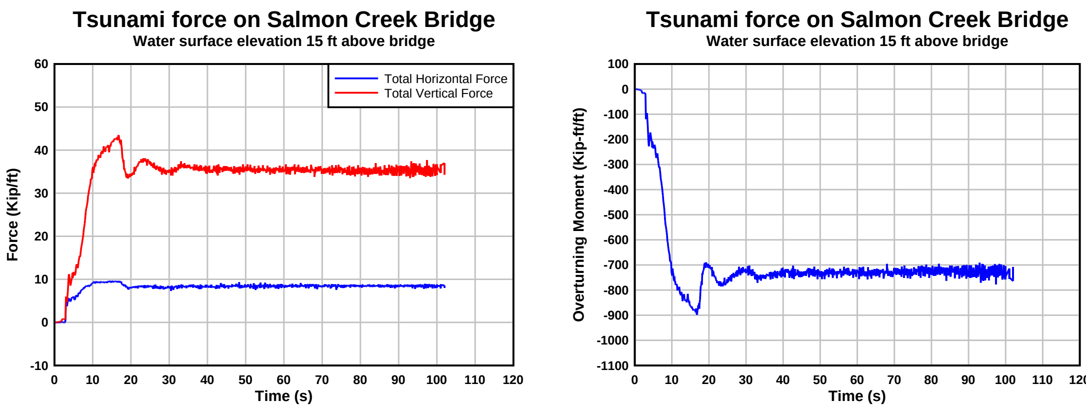

Figure 11. Tsunami force time history on the Salmon Creek Bridge, Water surface elevation 15 ft above bridge elevation

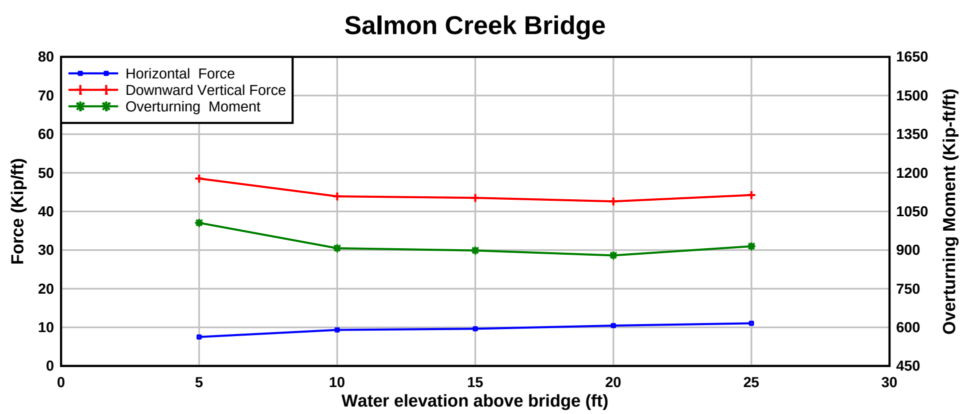

Figure 12. Maximum horizontal and vertical forces and overturning moment on Salmon Creek Bridge for five different water elevations

3. Malibu Lagoon Bridge

The Malibu Lagoon Bridge is a box-girder bridge with elevation approximately 16 foot - 4 inches above MSL. A total of five simulations were performed for this bridge, meaning that all four different time periods occurred at the same time. A set of screen captures of the simulation of Malibu Lagoon Bridge for water surface elevation of 10 ft above bridge elevation are provided in Figure 13. Figure 14 shows the tsunami force time history on the Malibu Lagoon Bridge for the scaled tsunami water free-surface elevation of 10 ft above bridge elevation. According to the results shown in this figure, there is a sudden increase in horizontal force due to initial impact on the bridge. This horizontal force gradually increases until the whole bridge is inundated resulting in relatively constant drag force. The behavior of the vertical force is slightly different. Although there is a sudden increase in vertical force in first few seconds due to initial impact on bridge, but as soon as the bridge starts to be inundated a large uplift force comes into picture reducing the downward vertical force. After the bridge is fully inundated no significant change in resulting vertical force was recorded. The behavior of horizontal and vertical forces for other four water surface elevations is practically identical.

Figure 15 shows the maximum horizontal and vertical forces and overturning moments on Malibu Lagoon Bridge for five different water elevations. According to the figure, both horizontal and vertical forces gradually increase with the water elevation although there is not a significant difference between results. It should be mentioned that in two of the simulations, water elevations 20 and 25 ft above bridge elevations, uplift forces were recorded at the end of the simulations where the bridge was fully inundated and water velocity was gradually decreasing. It is concluded that since the bridge is fully inundated and input water velocity is decreasing, the slamming force caused by water overtopping the bridge is not enough to overcome the uplift force.

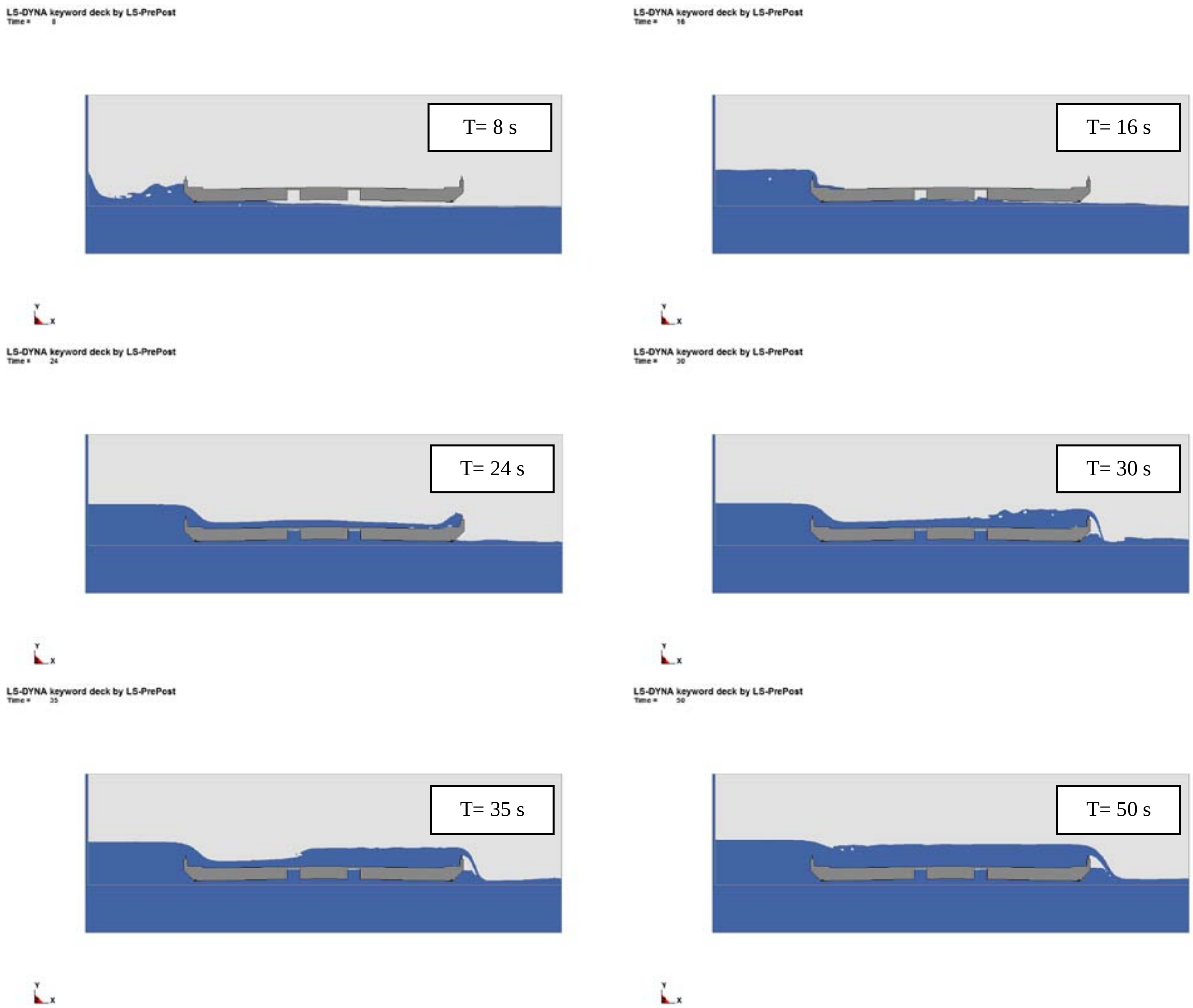

Figure 13. Screen captures of Malibu Lagoon Bridge, Water surface elevation 10 ft above bridge elevation

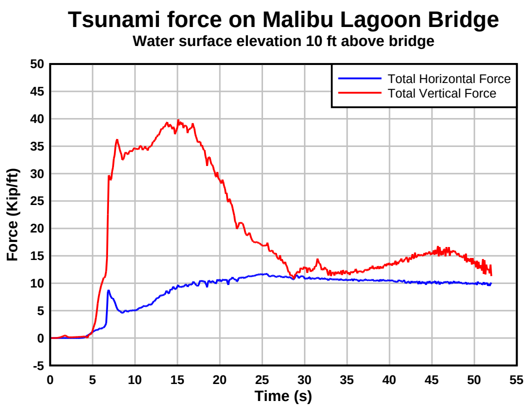

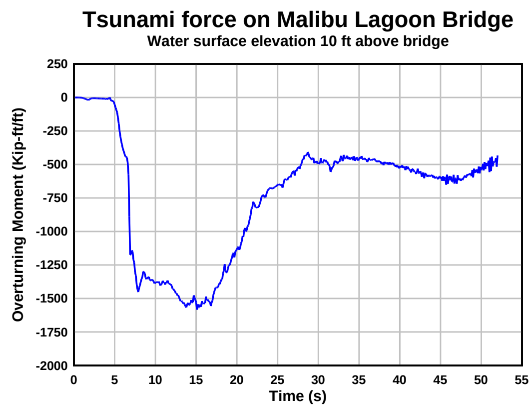

Figure 14. Tsunami force time history on the Malibu Lagoon Bridge, Water surface elevation 10 ft above bridge elevation

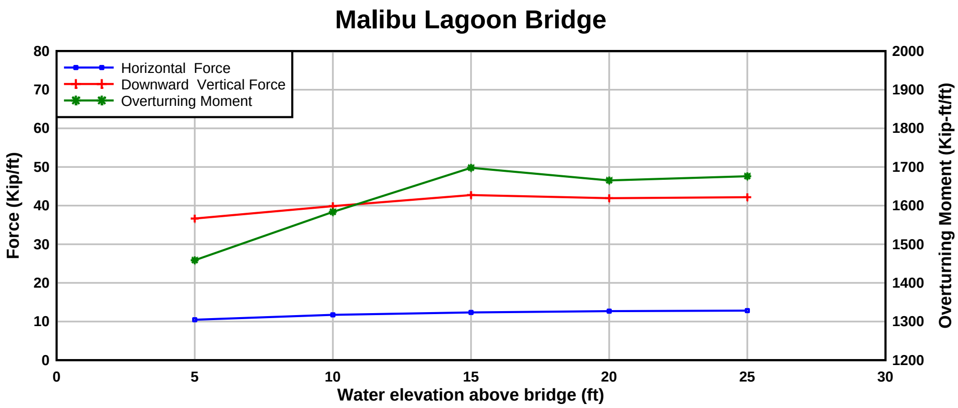

Figure 15. Maximum horizontal and vertical forces and overturning moment on Malibu Lagoon Bridge for five different water elevations

Concluding Remarks

This paper presented the preliminary results of an ongoing study on tsunami loading on three selected coastal bridges in California. The tsunami force time histories were computed for five different tsunami water surface elevations representing five tsunami scenarios. For each tsunami scenario four time periods were studied.

It was observed that maximum horizontal and vertical forces did not increase significantly by increasing the water surface elevation for box-girder bridges. The resulting maximum horizontal and vertical forces on the deck-girder bridge changed drastically for three lower water surface elevations. It was also found that bridges with relatively tall end barriers were prone to higher horizontal and vertical forces. Tsunami scenarios with higher water surface elevations generated higher horizontal forces. This increase in resulting horizontal force could be affiliated to both higher water velocity and higher hydrostatic pressure.

It was observed that maximum horizontal and vertical forces were in the same order for higher water elevations. The results also showed that initial impact on the bridge could generate larger vertical forces while the horizontal drag forces calculated in maximum momentum flux, velocity, and elevation times velocity time period were larger than corresponding forces in initial impact time period.

Another observation was that vertical forces were approximately 2 to 4 times larger than corresponding horizontal forces. It was concluded that one of the most important differences between tsunami and wind-generated waves such as hurricanes is the direction of the resulting vertical force. Tsunamis, due to a completely different generation source than wind waves, act like a traveling column of water while wind-generated waves are oscillatory and steady state. Wind-generated waves have much shorter time periods and lower maximum water surface elevations compared to tsunami waves. Short time period feature limits the time during which water overtops the bridge superstructure and consequently leads to less downward force. In this case, due to low water surface elevation, water hits the structure from beneath creating upward slamming force. This rise in water free-surface level may also lead to complete inundation of the bridge resulting in uplift force due to hydrostatic pressure difference between top and bottom of the bridge superstructure.

For tsunamis, due to very large time period on the order of hours, the time period during which the water overtops the bridge superstructure is relatively long resulting in high downward forces. Fortunately, this downward force is often beneficial in cancelling the uplift force which is one of the most important forces causing failure to connections between pile caps and girders. Thus it may be concluded that the failure of bridge superstructure in tsunamis is mainly due to large horizontal force caused by both high static pressure due to presence of a huge wave and also slamming force caused by the associated large wave velocity.

Finally, it is essential that the results and conclusions derived from this and similar numerical studies (including those of the Oregon coastal bridges over the past few years) be validated by large-scale experiments to assess their predictive capability and ranges of variability.

Acknowledgment

Partial support from the California Department of Transportation (Caltrans) is gratefully appreciated.

References

Cheung, K.F., Wei Y., Yamazaki Y., and Yim S.C., "Modeling of 500-year Tsunamis for Probabilistic Design of Coastal Infrastructure in the Pacific Northwest". Coastal Engineering, 2011: 970-985.

Douglass, S.L., Chen Q., and Olsen J.M. "Wave Forces on Bridge Decks," Washington: Federal Highway Administration, 2006.

Iemura, H., Pradono, M.H., Takahashi, Y., "Report on the tsunami damage on the bridges in Banda Aceh and some possible countermeasures," Proc. of 28th JSCE Earthquake engineering symposium, 2005.

LS-DYNA, 2010. Keyword User's Manual. Version 971, Revision 5. Livermore Software Technology Corporation, Livermore, California.

Nimmala, S.B., Yim S. C., Cheung K.F., Wei Y., “Tsunami Design Criteria for Coastal Infrastructure: A Case Study for Spencer Creek Bridge, Oregon”. Report prepared for Oregon Department of Transportation (ODOT). 2006

Padgett, J., DesRoches, R., Nielson ,B., Yashinsky, M., Kwon, O., Burdette, N., and Tavera, E. “Bridge Damage and Repair Costs from Hurricane Katrina,” Journal of Bridge Engineering. 2008.

“Probabilistic Tsunami Hazard in California,” Report prepared for Caltrans/PEER. 2010

Robertson, I.N., Yim, S., Riggs, H.R., Young, Y.L. “Coastal bridge performance during Hurricane Katrina, Proc.,” Structural Engineering, Mechanics and Computation 3,pp. 1864-1870, 2007.

Robertson, I.N., Riggs, H.R., Yim, S.C.S., Young, Y.L. “Lessons from Hurricane Katrina storm surge on bridges and buildings,” Journal of Waterway, Port, Coastal, and Ocean Engineering, Vol. 133, pp. 463-483, 2007.

Yim, S. C., Cheung, K.F., Boon-intra S., Winston H. M., Nimmala S.B., Azadbakht M., and Wei Y. “Estimation of Tsunami Loads on Bridge Superstructure in the Pacific Northwest”. in progress.

Yim, S. C., Boon-intra S, Nimmala S.B., Winston H. M., Azadbakht M., Cheung K.F., “Development of a Guideline for Estimating Tsunami Forces on Bridge Superstructures” Report prepared for Oregon Department of Transportation (ODOT). 2011.

Yashinsky, M. Lessons for Caltrans from the 2011 great Japan earthquake and tsunami, Proceedings of the International Symposium on Engineering Lessons Learned from the 2011 Great East Japan Earthquake, March 1-4, 2012, Tokyo, Japan.